Bernoulli catenary and elasto-capillary effect in partially wet fibrous materials

Daria Monaenkova, Taras Andrukh and Konstantin G Kornev

Textile Research Journal published online 3 June 2013
DOI: 10.1177/0040517512464294

Original article

Textile Research Journal
0(00) 1–12

DOI: 10.1177/0040517512464294
trj.sagepub.com

Bernoulli catenary and elasto-capillary effect in partially wet fibrous materials

Daria Monaenkova, Taras Andrukh and Konstantin G Kornev

Abstract

When a wetting liquid wicks into a fibrous material, it causes the material to deform. In this paper we discuss the elasto-capillary effect that leads to spontaneous internal stresses in the materials. The elasto-capillary effect produced by menisci in pores can be identified through a specific stress distribution in the fibrous matrix. We show that the classical Bernoulli problem of a freely hanging fabric can be used for the analysis of gravity-induced stresses in textile materials. These stresses change due to elasto-capillary effect. Wicking of a wetting liquid into a freely suspended fibrous material is shown to be an instructive nontrivial experiment illustrating interesting distinguishable stress distributions in the fibrous matrix.

Keywords

fibrous materials, elasto-capillarity, catenary, wicking, stress analysis

A saturated textile material can be considered as a complex composite, which implies that any loading imposed on the material is shared between its fibrous network and saturating liquid.[1–4] As a result, mechanical and wicking effects are coupled. On the one hand, the wicking of the wetting liquid through the textile yarn or fabric is affected by the tensile loading imposed on the material.[5,6] On the other hand, the mechanical performance of the material depends on whether it is wet or dry.[7,8] In the general case, the effect of moisture on the operation of textile materials is a complex problem with multiple variables. In this paper we provide a detailed investigation of one of the multiple effects caused by the presence of liquid in the fibrous matrix.

The interactions of liquid menisci with fibers often lead to the variation of stress in the materials, manifested through the fabrics deformations, the so-called elasto-capillary effect.[9–11] The most vivid example of elasto-capillarity observed in everyday life is the coalescence of wet hair.[12] Other examples include buckling of carbon nanotubes exposed to the water vapor[13] and deformations of the nanoporous yarns transporting the wetting liquids.[14,15]

The level of stresses in wearable textiles due to the elasto-capillary effect[15] is comparable with stresses which fabric encounters during its daily use.[6,16] Since the mechanical properties of textile material is one of the key features affecting the material performance,[6] an understanding of the influence of the liquid on the stressed state of the wetted fabric is important.

In our recent paper[17] we have discussed a problem of liquid flow through a freely suspended fibrous material. In the experiment, the liquid driven by capillarity and hydrostatic forces wicks along the sample, which continuously adjusts its shape according to the level of saturation (Figure 1(a)). Although the kinetic problem was studied in details, the elasto-capillary problem was

School of Materials Science and Engineering, Clemson University, Clemson, SC, USA

Corresponding author:
Konstantin G. Kornev, School of Materials Science and Engineering, 161 Sirrine Hall, Clemson University, Clemson, SC 29634, USA.
Email: kkornev@clemson.edu

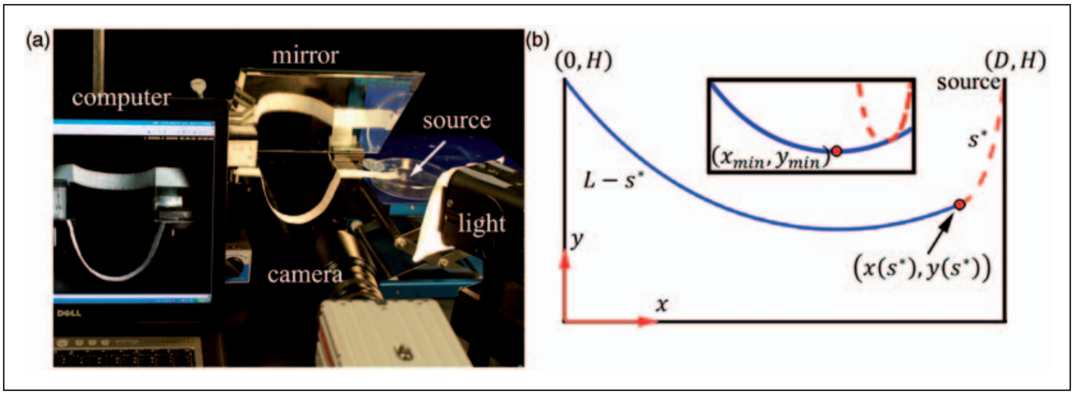

Figure 1. (a) Experimental setup: sample absorbs liquid from the left. The color variation allows to us distinguish between wet and dry parts of the sample. The front position is observed in a mirror installed above the sample. A camera is used to record the front position and the corresponding sample profile. (b) The shape of the partially wet fabric of length L. The fabric absorbs a liquid from the source positioned at the top of the right post, (D,H). The liquid (dotted line) wicks into the fabric and changes its shape. The position of the wetting front is s^*. Inset: Two catenaries describing the dry and wet parts of the fabric.

not examined. In this paper we discuss the elasto-capillary effect in the freely suspended materials and provide a full analysis of stresses acting on the fibrous network upon liquid invasion. It will be shown that the tensile stresses caused by gravity can be reduced by capillary compression experienced by the fibrous network during the liquid flow. The strength of the capillary compression is qualitatively discussed using two parallel metal wires, which are visually deformed by the wicking liquid.

Unlike fiber rails, densely packed fabrics are difficult to deform in plane: each fiber is held in place at the crossing points where the fiber is subject to extremely strong friction.[18] When liquid wicks in a planar sample, the tensions in the fibrous network are hidden. These tensions can be visualized through deformations of the sagged samples. Tracking the changes of the sample profile, we study the evolution of stresses acting on the fibers in both the dry and wet parts of the sample at different saturation levels.

Modeling deformations of the sagged fabrics we assume that the material does not change its length, but, owing to its flexibility, takes on any shape dictated by gravity. In this respect, the material is very similar to a hanging chain sagged under its own weight. To describe the shape of the freely suspended sample we modified a theory proposed by Bernoulli,[19] which is often used to describe the shape of many engineering constructs.[20,21] In this paper, the Bernoulli theory is applied to examine the stresses in freely suspended fabrics semi-saturated with wetting liquids. The results on wicking kinetics in these fabrics have been discussed in our recent paper.[17] The main parameters of the experiment (see Figure 1(b)) are summarized in Table 1. In the Appendix, we describe the experimental conditions in detail.

Theory

Distinguishable elasto-capillary effect in fibrous samples

In fibrous materials, the applied stresses are distributed over the matrix and saturating fluid. Therefore, when one part of the material is wet and another is dry, the stresses acting upon the fibers in wet and dry parts of the specimen differ. Poroelasticity theory can be applied for the analyses of wet fabrics.[2–4] Here we consider a rectangular nonwoven material such as a strip of paper or a piece of fabric clamped from one edge and subjected to a tensile force F^- from the other (Figure 2(a)). We assume that the force is distributed uniformly over the edge. Here and throughout, the parameters of the problem related to the dry material we denote with a 'minus' superscript and to the saturated material with a 'plus' superscript.

In-plane stresses. In the dry sample, we can write the force balance as $F^- = \sigma^- A_\perp$, in which σ^- is the in-plane stress acting over the edge cross-section. Assuming that the atmospheric pressure is set to zero, we can say that this stress is supported only by the fibers. We can also introduce an average stress exerted on each fiber, T^- (see Figure 2(b)). The force balance can be rewritten as

$$F^- = \sigma_\perp^- A_\perp = T_\perp^- (1 - \varepsilon_\perp) A_\perp \tag{1}$$

where $\varepsilon_\perp = A_\perp^{\mathrm{p}} / A_\perp$ is the ratio of cross-sectional area of pores to the total cross-sectional area of the sample.

In the wet samples subject to the same load, the average normal stress is supported by the liquid

Table 1. Characteristics of the samples used in experiments

L (cm)	D (cm)	H (cm)	h (μm)	w (cm)	ρ^+/ρ^-	k (D)	$\varepsilon_\perp$	R_p (μm)
17	9.54	9.17	300	2	10	230	0.91	152

L, length of the sample between suspension points; D, distance between two posts; H, height of the posts; h, sample thickness; w, width of the sample; ρ^+/ρ^-, ratio of the linear densities of the wet and dry sample; k, sample permeability; $\varepsilon_\perp$, trans-plane porosity of the sample; R_p, pore radius in the material (see Figure 1(b)).

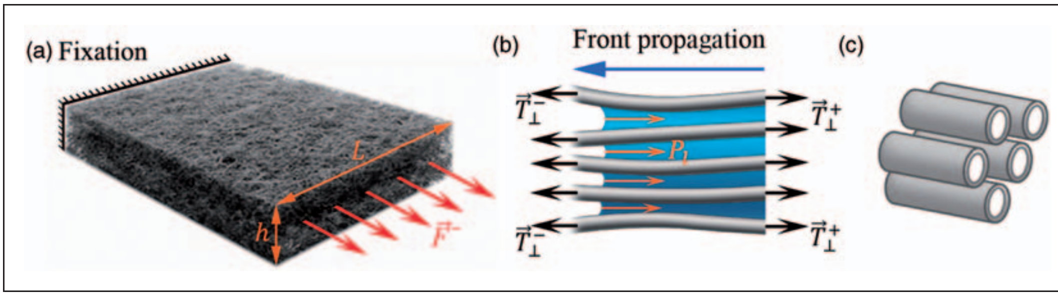

Figure 2. (a) Fibrous material subjected to tensile loading. (b) Stress distribution in a semi-saturated sample. (c) A fabric made of bundles of hollow fibers.

and fibers.[15] Again, the force balance is written for the wet sample as

$$F^+ = \sigma_\perp^+ A_\perp = T_\perp^+(1-\varepsilon_\perp)A_\perp - P_l\,\varepsilon_\perp A_\perp \qquad (2)$$

where $\sigma_\perp^+$ is the average in-plane stress acting on the wet sample, $T_\perp^+$ is the tensile stress experienced by each fiber, and P_l is the pressure in the liquid, sometimes called the pore pressure.[2–4] The compressive pressure is considered positive.

In the mechanics of porous materials, parameter $\varepsilon_\perp$ is considered identical to the sample porosity, i.e. the ratio of pore volume to the sample volume.[2–4] However, it is not obvious whether or not we can apply this interpretation to fibrous materials. For example, if a fabric is made of bundles of hollow fibers as schematically shown in Figure 2(c), parameter $\varepsilon_\perp$ in force balance (2) contains the integral cross-sectional area of tube openings as well as the area of interfiber openings. If one places a fabric on water and seals the fabric edges, water will flow perpendicularly to the fabric surface leaving the holes in the fibers empty. Thus, the theory should distinguish these two cases by introducing two parameters, $\varepsilon_\perp$ and $\varepsilon_{||}$, where $\varepsilon_{||}$ is the ratio of the in-plane area of pores $A_{||}^{p}$ to the total in-plane area $A_{||}$ of the sample.

The pressure term, Equation (2), permits an elucidation of the elasto-capillary effect. The stresses caused by spontaneous wicking of a wetting liquid into a sample illustrate the differences between the stress state in both dry and wet materials. Assume that the sample is subject to tensile force F^- and the liquid invades the sample from the loaded side. When the liquid wicks into the material, it forms a wetting front separating dry and wet parts. One can immediately infer that the same force F^- is supported by the stresses $\sigma_\perp^-$ and $\sigma_\perp^+$, $F^- = \sigma_\perp^- A_\perp = \sigma_\perp^+ A_\perp$. Solving Equations (1) and (2) for the fiber stresses, we obtain $T_\perp^- = F^-/\,[(1-\varepsilon_\perp)A_\perp]$ and $T_\perp^+ = (F^- + P_l\varepsilon_\perp A_\perp)/[(1-\varepsilon_\perp)\ A_\perp]$. Since there is no trans-plane flow through the sample thickness, the pressure P_l is constant in each cross-section, and it is merely a local capillary pressure induced by the menisci exposed to the atmosphere. Concave menisci formed by wetting liquids produce a negative pressure in the liquid, $P_l < 0$. We thus conclude that tension $T_\perp^+ = (F^- + P_l\varepsilon_\perp A_\perp)/[(1-\varepsilon_\perp)A_\perp]$ on the wet fibers is always smaller than tension $T_\perp^- = F^-/[(1-\varepsilon_\perp)A_\perp]$ on the dry fibers. Thus, the stronger the suction pressure in the liquid, the greater the difference between $T_\perp^-$ and $T_\perp^+$. In this paper all conclusions are derived for the in-plane stresses if not mentioned otherwise.

Trans-plane stresses. Similar arguments are applicable to the analysis of trans-plane stresses. As follows from the force balance in the dry band, $F^- = A_{||}\sigma_{||}^- = (1-\varepsilon_{||})\ A_{||}\ T_{||}^- = 0$, where $\sigma_{||}^-$ is the trans-plane stress acting at the sample surface. Therefore, the stress on fibers is zero. However, in the wet part, the trans-plane stress on fibers is not zero: $T_{||}^+ = P_l\ \varepsilon_{||}/(1-\varepsilon_{||})$. For example, in wicking experiments, the pressure in the liquid causes a negative compression of the sample in the transverse direction through its thickness. Therefore, capillary forces acting through the sample thickness tend to

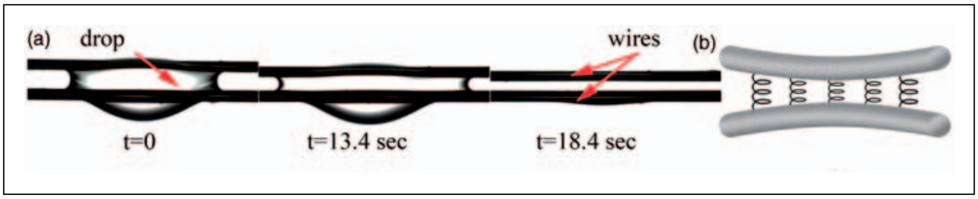

Figure 3. (a) Droplet of Galwick absorbed by the fiber rails composed of two tungsten wires. Observe the contraction of interfiber gap when the drop transforms into a liquid bridge with concave menisci. The thickness of the interfiber space at the first moment is 128 μm which then changes to 67 μm after drop spreading. (b) Mechanical model of the elasto-capillary effect.

bring fibers closer together as evidenced in experiments with two fiber rails.

In order to appreciate the strength of the capillary forces, in Figure 3(a) we show the results of experiments on drop spreading over a channel composed of two freely suspended tungsten wires. The 70 μm diameter wires of 7.4 cm length were stretched straight and firmly clamped to two solid bars. In order to separate the wires and preserve the interwire spacing, two 1.5 mm diameter pins were placed between the wire ends. A Galwick drop (PMI Inc, Ithaca, NY) with surface tension $\gamma = 15.6$ mN/m was placed at the center of the wire rails. As the drop spread and filled the interwire gap, we observed the gap contraction. The visible deformation of the stretched wires suggests that the capillary pressure P_c created by the menisci, forces the fibers to snap off the gap between them. As clearly seen from experiments on hair strands[12] and wire rails, the internal tension on the fibers is significant. Figure 3(b) represents a mechanical model of this elasto-capillary effect, in which the springs modeling the capillary forces, pulling the wires in close proximity to each other.

This work is focused mainly on the in-plane stresses, since in the dense fibrous samples the transverse deformations are hardly detectable. Equations (1) and (2) in general can be applied for the analysis of the stresses experienced by the fibers in semi-saturated materials.

When the tensile forces $F^{\pm}$ acting on dry and wet cross-sections are found and the pressure P_l in the wetting liquid is known, then the tension T^+ on the fibers of the saturated matrix relatively to the tension T^- in the dry sample can be estimated. In the general case, F^+ may differ from F^-. As we show below the value of the tensile force in each cross-section can be extracted from the shape of the freely suspended semi-saturated sample.

Fabric profile and forces acting on wet and dry parts

The shape of a fabric freely suspended between two posts of the equal height H is controlled by the weight distribution over the fabric. In the simplest cases, the fabric is either completely wet or dry. In more complex situations considered in this paper the samples are semi-saturated (see Figure 4(a)). The force balance equations for any small segment of the freely suspended fabric (Figure 4(b), inset) reads as

$$\frac{d}{ds}\left(F\frac{dx}{ds}\right) = 0, \quad \frac{d}{ds}\left(F\frac{dx}{ds}\right) = 0 \tag{3}$$

where $\rho = \rho(s)$ is the linear mass density of the fabric, s is the arc length, g is acceleration due to gravity. As follows from the first expression of Equation (3) and the continuity condition, the x-component of tensile force remains constant along the fabric.[22]

The force balance equations (Equations (3)) are valid for the samples with uniform weight distribution as well as for samples where the linear density changes as a step function (for examples see Figure 4(a) and (b)). The last situation can be achieved in experiments, where a freely suspended sample absorbs liquid from one end. For such situation, following the analysis of Bernoulli[19] and Freeman,[23] and integrating the second expression of Equation (3),[17] one can show that the sample profile can be defined using a combination of catenary equations describing dry and wet parts of the sample (Figure 1(b), inset):

$$\begin{aligned} &y^- = a^-\cosh\left(x - x^-_{min}\right) + Y^-, \ 0 < x^- < x(s^*), \\ &\quad \text{and } y^+ = a^+\cosh\left(x - x^+_{min}\right) + Y^+, \\ &\quad x(s^*) < x^- < D, \end{aligned} \tag{4}$$

where s^* is the front position, $a^{\pm} = \frac{F_x}{\rho^{\pm} g}$ are the shape factors, ρ^- and ρ^+ are linear densities of the dry and wet parts of the material, F_x is the horizontal component of tensile force along the sample profile $\left(x^{\pm}_{min}, Y^{\pm} + a\right)$ the coordinates of catenary minimum describing dry "–" or wet "+" parts of the sample, 0 and D denote the horizontal coordinates of the suspension points.

The simultaneous application of the force balance equation (Equation (3)) and explicit form of the

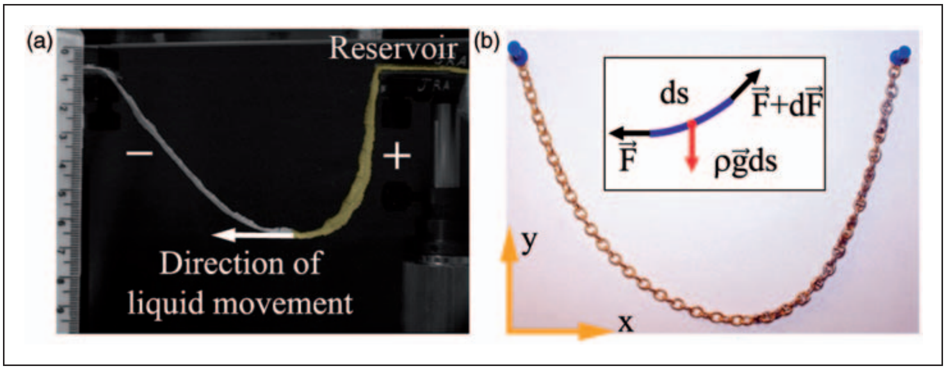

Figure 4. (a) Partially saturated freely suspended fibrous sample. (b) Freely suspended chain composed of two types of the links. Right links are heavier, which causes profile asymmetry. Inset: The force balance for an elementary piece of the freely suspended sample of arclength *ds*, ρg is the weight per unit length of the sample, *F* and $F + dF$ are the stresses acting at the edges of the element.

catenary equation (Equation (4)) allows one to find the tensile forces acting along the dry and wet parts of the fabric. These forces are expressed as

$$F^{\pm} = a^{\pm}\rho^{\pm}g \cdot \cosh\left(\left(x - x^{\pm}_{min}\right)\right)/a^{\pm} \quad (5)$$

Hyperbolic cosines are expressed from Equation (4), yielding the following equations for the forces

$$F^{-} = \rho^{-}g(y^{-} - Y^{-}) \text{ and } F^{+} = \rho^{+}g(y^{+} - Y^{+}) \quad (6)$$

Therefore, the total force acting on each cross-section is linearly proportional to its vertical coordinate and a coefficient of proportionality is related to the linear density of the sample at this point. The unknown parameters $a^{\pm}$, $x^{\pm}_{min}$, $Y^{\pm}_{min}$ can be found from the boundary conditions and the front position s^* is obtained by numerical integrating the kinetic equation as discussed elsewhere.[17]

The pressure in the moving liquid column is a combination of the hydrostatic and capillary pressure and reads[17]

$$P_l = -\left[P_c + \rho_l g(H - y^{+}(s^*))\right] \cdot s/s^* + \rho_l g\left(H - y^{+}(s)\right) \quad (7)$$

This equation was derived from Darcy's law[15] and implies that the pressure in the liquid column drops linearly from zero at the liquid source, $s = 0$, to $-P_c$ at the wetting front, $s = s^*$. The impregnation of nanoporous materials is driven mostly by the capillary pressure,[24–26] i.e. the effect of gravity in Equation (7) can be safely neglected. However, in materials with micrometer or larger pores, one has to take into account both effects in Equation (7). The capillary pressure is a characteristic function of the given fibrous material and is defined as the difference between the atmospheric pressure and pressure in the menisci forming the wetting front.[1] Modeling the fibrous material as a bundle of capillaries, the capillary pressure can be estimated as $P_c \sim 2\gamma \cos\theta/R_p$, where γ is the interfacial tension of the liquid/air pair, R_p is the characteristic pore radius, and θ is the contact angle that the liquid forms with the pore wall. We discuss only wicking of wetting fluids, hence we assume that the contact angle is zero. The parameters of the material such as porosity, pore size, permeability, and linear density used for the calculations are given in Table 1. The wicking liquid in the model is water.

Dynamics of fabric sway

As follows from the transcendental equation for the shape factor, $L/(2a) = \sinh(D/2a)$, if the geometry of the experiment is identical for the heavy and light samples, i.e. parameters H, D, L are identically maintained, the sample profiles will also be identical. Although these profiles are completely described by a single shape factor a, the tension on these materials is different. This is the fundamental property of catenaries: heavy chains and light yarns of the same length would acquire the same configuration. Therefore, if liquid wicks into the hanging fabric from one end, the profile changes, but the final configuration of the wet fabric is the same as the initial dry configuration.

Since the wet part of the sample is always heavier than the dry part, one would expect that the liquid wicking would cause the sample deflection toward the post that supports the liquid source. We conducted a numerical analysis of the sway of a fabric fixed between two posts of the equal height. The geometry is chosen as discussed in the Appendix 1 and Table 1. A numerical analysis of the model shows that the longer the wet part of the sample, the larger the deviation of the sample profile from its initial symmetric

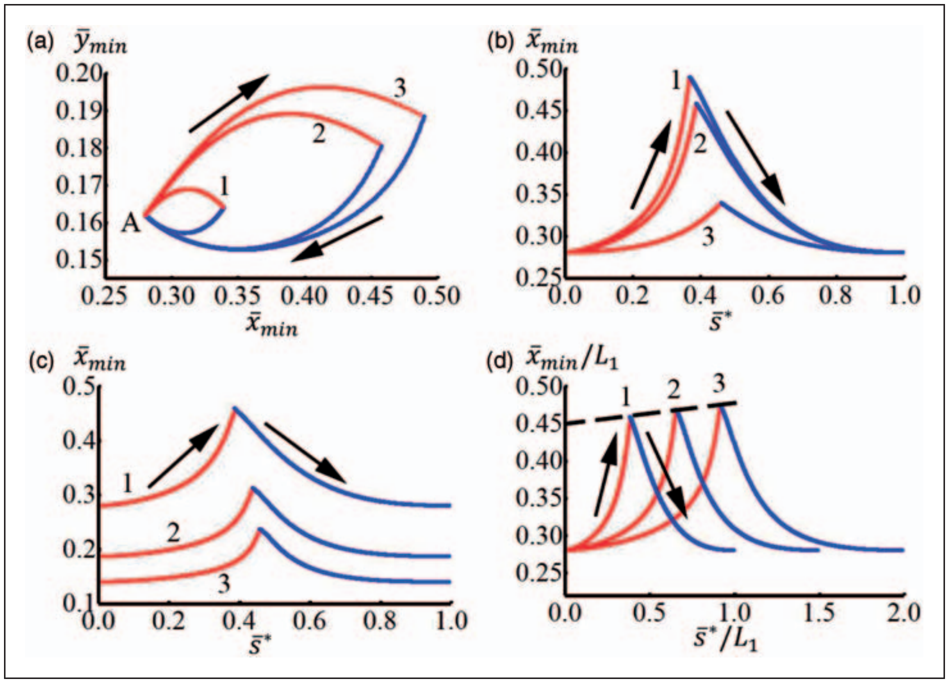

Figure 5. (a) Position of the sample minimum during the wicking experiment. The upper branches correspond to the downward wicking, while the lower branches correspond to the upward wicking. The corresponding ratio of linear densities of the material in dry and wet state in these experiments is $\rho^+/\rho^- = 20$ (1), $\rho^+/\rho^- = 10$ (2) and $\rho^+/\rho^- = 2$ (3). (b) x-coordinate of the minimum of the sample profile plotted versus the position of the wetting front. The corresponding ratio of linear densities of the material in both the dry and wet state in these experiments is $\rho^+/\rho^- = 20$ (1), $\rho^+/\rho^- = 10$ (2) and $\rho^+/\rho^- = 2$ (3). (c) x-coordinate of the minimum of the sample profile plotted versus position of the wetting front s^* along the sample, normalized by sample length L. The graph shows the results for three samples with different lengths: L_1:L_2:$L_3 = 1$:1.5:2. The longer the sample the longer is the wet part $\bar{s}^*$ required to change the direction of the sway. (d) Horizontal position of the minimum of the sample profile plotted versus normalized front length $\bar{s}^*$. The graph shows three experiments with samples of different lengths: $L_1 : L_2 : L_3 = 1$:1.5:2. The front position along the sample is normalized by the length of the shortest sample L_1. Dashed line shows the shift of x_{min} due to increase of the sample length.

configuration. The sample swings back to restore its initial symmetry when the wetting front passes the profile minimum (x_{min}, y_{min}). The calculated phase portrait (x_{min}, y_{min}) is shown in Figure 5(a).

The profile of a partially wet fabric is specified by the ratio of linear densities of the material in the dry and wet parts expressed as $a^+/a^- = \rho^-/\rho^+$. This ratio defines the size of the hysteresis loops, generated in the XY plane. Moreover, this ratio defines the sway of the sample from its symmetric configuration (Figure 5(a) and (b)). The analysis of the Bernoulli model reveals that the heavier the wet sample, the less is the length of the wet part of the sample, s^*, at which the sample begins to restore its symmetry. Also, the heavier the liquid, the greater the sway of the sag.

The dependence of the fabric sway on its length L is shown in Figure 5(c) and (d). The longer the sample, the bigger its sway. Moreover, the length of the wet part corresponding to the moment when the fabric starts to sway back increases together with the fabric length.

Summarizing the modeling results, we conclude that the heavier the liquid or the longer the sample, the greater its deflection from the initial profile during wicking experiments. However, the heavier the liquid, the faster it will bring the sample to its symmetric configuration. Conversely, however, the longer samples would require the longer wet part to reverse the sample movement.

Tensile forces in the freely suspended samples

Force analysis for dry and wet samples. The shape of the freely sagged sample contains valuable information about forces $F^{\pm}$ acting along the sample profile (Equation (4)). According to momentum balance[23] these forces are tangential to the sample profile and their magnitudes are proportional to the vertical coordinate $y^{\pm}$ of the cross-section in question (Equation (4)). The coefficient of proportionality depends on the linear density of the sample $\rho^{\pm}$, and the total tensile force at each cross-section consists of two components, $F_y^{\pm}, F_x^{\pm}$. To describe the force change along the sample profile, we discuss the behavior of vertical, $F_y^{\pm}$, and horizontal, $F_x^{\pm}$, components separately.

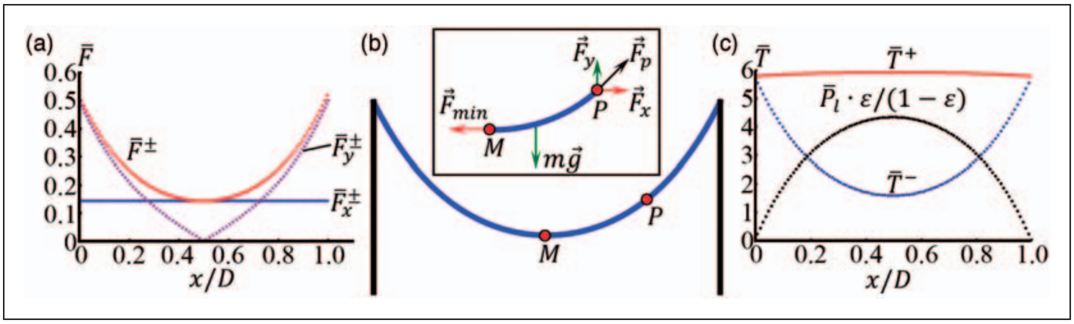

Figure 6. (a) The tensile force $\bar{F}^{\pm}$, and the horizontal $\bar{F}_x^{\pm}$ and vertical components $\bar{F}_y^{\pm}$, act along the profile of a completely wet/dry sample, normalized by the weight of the sample $\rho^{\pm}gL$. (b) Sample with uniform weight distribution. *M* is the lowest point of the profile. *P* is an arbitrary point. Inset: free body diagram for segment *MP*. (c) Tensions experienced by fibers in completely dry $\bar{T}^{-}$ and completely wet $\bar{T}^{+}$ samples normalized by $\rho^{\pm}gL/S$ and pressure in the liquid in a completely wet sample $\bar{P}_l \cdot \varepsilon_{\perp}/(1-\varepsilon\perp)$ (equation 7) normalized by $\rho^{+}gL/S$. All parameters are taken from Table 1.

For a reference, consider the distribution of forces acting upon the dry sample with a constant linear density of ρ^- (Figure 6(a)). As follows from Equation (3), the derivative of the x-component is zero, $dF_x^-/ds = 0$, therefore implying a constant in this force component $F_x^- = const$. This constant is equal to the total force $F^-(x_{min,}y_{min})$ acting at the lowest point of the sample profile, $M(x_{min,}y_{min})$, where the vertical force component is zero. The vertical component F_y^- depends upon s, $dF_y^- = \rho^- gds$. To find F_y^- acting at arbitrary point $\mathrm{P}(x_{p,}y_p)$ we consider the free body diagram shown in Figure 6(b). Forces $\vec{F}^p$ and $\vec{F}_{min}$ act at the end-points of the piece of fabric shown in Figure 6(b). The weight of the segment MP, $\vec{W}_{MP}$, is applied to the center of mass of this segment MP and is directed downward parallel to the y-axis. If ρ^- is a linear density of the dry sample, then the weight of MP is $\vec{W}_{MP} = \rho^-(s_{min} - s_p)\vec{g}$, where s_{min} and s_p are the arclengths of points M and P, respectively. The force balance is written as

$$F_x^-(x_{p,}y_p) = F^-(x_{min,}y_{min}), F_y^-(x_{p,}y_p) = \left|\vec{W}_{MP}\right| = \rho^-(s_{min} - s_p)g$$

Therefore, the vertical force component $F_y^-(x_{p,}y_p)$ acting at point P is equal to the weight of the segment MP. If point P is closer to the left post $\mathrm{s_p} > \mathrm{s_{min}}$, then this force is written as $F_y^p = \rho^-(\mathrm{s_p} - \mathrm{s_{min}})\mathrm{g}$. The same results can be obtained by integrating the force balance (Equation (3)), $dF^y = \rho^- g d\mathrm{s}$, over the segment MP.

For completely wet and dry samples the distribution of tensile force normalized by the sample weight is identical, $F^{\pm}/\rho^{\pm}g = (y^{\pm} - Y^{\pm})$. However, the stresses experienced by fibers in the wet and dry samples differ. In the case of the completely wet material the pressure in the liquid is $P_l = \rho_l g(H - y^+)$. Substituting this pressure in Equation (2), we see that the tension on the fibers differs greatly from the force acting upon the catenary as a whole. In Figure 6(c) we show the tensions acting upon the fibers along the dry and wet catenary. In the absence of capillary pressure in the liquid, the hydrostatic pressure in the liquid column acts to stretch the fibrous matrix. This extra tension increases from the liquid source to the saddle point of the sample profile and, as a result, the tension on fibrous skeleton remains almost constant (Figure 6(c)).

Horizontal force component. A partially wet catenary adjusts its shape so that the forces acting along it would satisfy two conditions: (a) the horizontal component of the tensile force in wet and dry parts should be equal to each other $F_x^+(s^*) = F_x^-(s^*)$; and (b) at the wetting front, the forces change continuously without any jump, $F^+(s^*) = F^-(s^*)$. The condition (a) immediately provides a relationship between the shape factors, $F_x^{\pm} = \rho^{\pm}ga^{\pm} \Rightarrow a^+/a^- = \rho^-/\rho^+$. The horizontal component of the tensile force is the same at each cross-section and increases continuously as the front propagates through the sample (Figure 7(d)).

Vertical force component. As shown above, at arbitrary point P, the vertical component of the tensile force in completely dry or wet samples is defined by the weight of the MP segment (Figure 6(b)). Assuming that points M and P both belong to either the dry or wet parts of the sample, as in case (ii) or (iv) in Figure7(a), we can integrate Equation (3) to prove that the same conclusion is valid for a partially wet sample, $F_y^-(x_{p,}y_p) = |\vec{W}_{MP}|$. In these cases, $F_y^{\mp}(x_p, y_p) = \rho^{\mp}g|s_{min} - s_p|$ is applicable. The modulus makes the definition universal independently of whether $s_{min} > s_p$ or $s_{min} < s_p$.

When the front marked by $F(x(\mathrm{s}^*), y(\mathrm{s}^*))$ passes point P but does not yet reach point M, as in case (iii) in Figure 7(a), the integration of Equation (3)

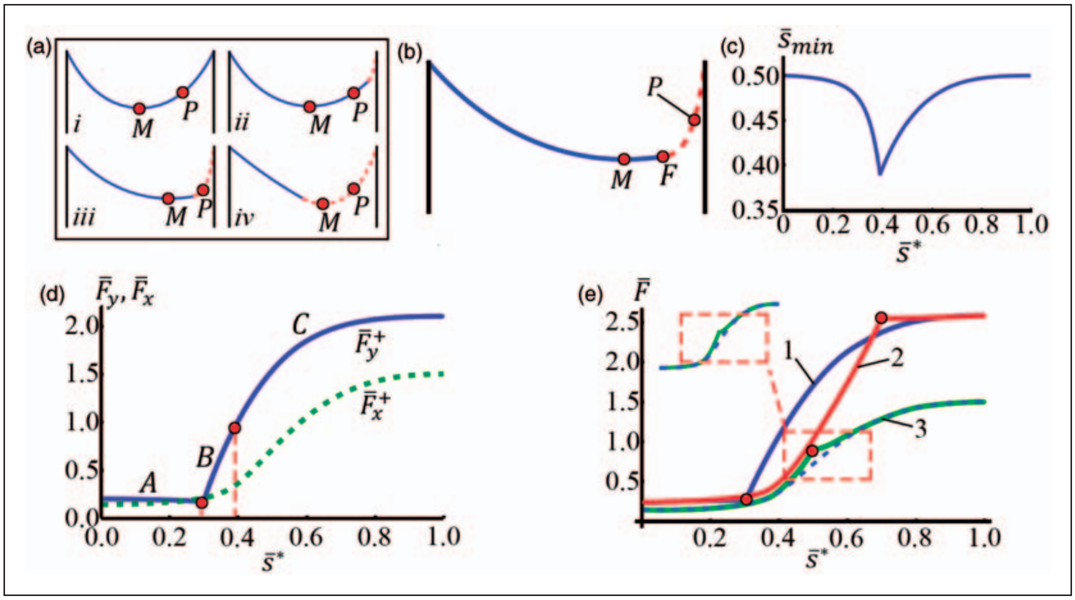

Figure 7. (a) Change of the relative position of the lowest point M and test point P of arclength $s_p = 0.3\,L$ during wicking experiments. (b) Schematic of the sample profile when the segment MP is partially wet; the dashed line shows the wet part. (c) Change of the arclength of point M, $\bar{s}_{min} = s_{min}/L$, as a function of the arclength of the wetting front, $\bar{s}^* = s^*/L$. (d) Change of vertical $\bar{F}_y^{\mp}$ and horizontal $\bar{F}_x^{\mp}$ components of the tensile force acting at the point $s_p = 0.3\,L$. Region (A): $s^*/L < 0.3$; region (B): $0.3 < s^*/L < s_{min}/L$; region (C): $s^*/L > s_{min}/L$. (e) Variation of the tensile force $\bar{F}$, acting at the points $s_p = 0.3\,L$ (1), $0.7\,L$ (2) and $0.5\,L$ (3). The dashed line shows the distribution of the horizontal force component $\bar{F}_x^-$. The inset shows the magnified portion of curve 3 at the region where the vertical force $\bar{F}_y^{\mp}$ corresponding to $s = 0.5\,L$ is the greatest. All forces $\bar{F}, \bar{F}_y^+, \bar{F}_x^+$, are normalized by the weight of the dry sample, $\rho^- gL$.

must be undertaken with a care. In this case, the catenary segment MP is partially wet (Figure 7(b)). The force balance can be written for dry part MF and wet part FP, separately: for part MF we have

$$F_x^+(x(s^*), y(s^*)) = F^-(x_{min}, y_{min}), F_y^-(x_f, y_f) = \rho^-(s_{min} - s^*)g;$$

and for part FP we obtain

$$F_x^+(x_p, y_p) = F_x^+(x(s^*), y(s^*)), F_y^-(x_p, y_p) = F_y^-(x_f, y_f) + \rho^+(s^* - s_p)g,$$

Substituting force $F_y^-(x_f, y_f)$, from the first line, the force balance is rewritten as $F_x^+(x_p, y_p) = F^-(x_{min}, y_{min})$, $F_y^-(x_p, y_p) = \rho^-(s_{min} - s^*)g + \rho^+(s^* - s_p)g$. Again, the y component of the force is equal to the weight of the segment MP. If $s_p > s_{min}$, we have for a partially wet sample $F_y^-(x_p, y_p) = \rho^+ g(s^* - s_{min}) + \rho^- g(s_p - s^*)$. When the front propagates through the sample, the arc length s_{min} of point M changes (see Figure 7(c)). If the segment MP is either completely wet or dry, this change of s_{min} is the only reason for an alternation of the vertical component of the force acting at point P. As the liquid moves deeper into the sample, the material becomes heavier and alters the vertical force component. As an example, we follow the changes of the vertical force component acting at $s(x_p, y_p) = 0.3L$ (Figure 7(d)).

Total force. The total force F^p acting on the sample cross-section can be expressed as $F^p = \sqrt{F_x^2 + F_y^2}$. While identical results can be obtained using Equation (6), the representation $F^p = \sqrt{F_x^2 + F_y^2}$ is more illustrative. Figure 7(e) shows a typical behavior of the tensile forces acting at $s_p = 0.3\,L$, $0.5\,L$ and $0.7\,L$. At the initial and last stages of the wicking, the tensions in the sample cross-sections located at the opposite sides of the sample are almost equal. As the weight difference between the sample segments in question is small, this equality occurs when the liquid just enters the sample and passes the second cross-section when the sample is almost filled. The tensile force acting on the cross-section located in the half of the sample length is almost defined by its horizontal component. The further the deviation of the cross-section from the initial symmetrical position, the higher the weight between the lowest point M and this cross-section becomes, with a

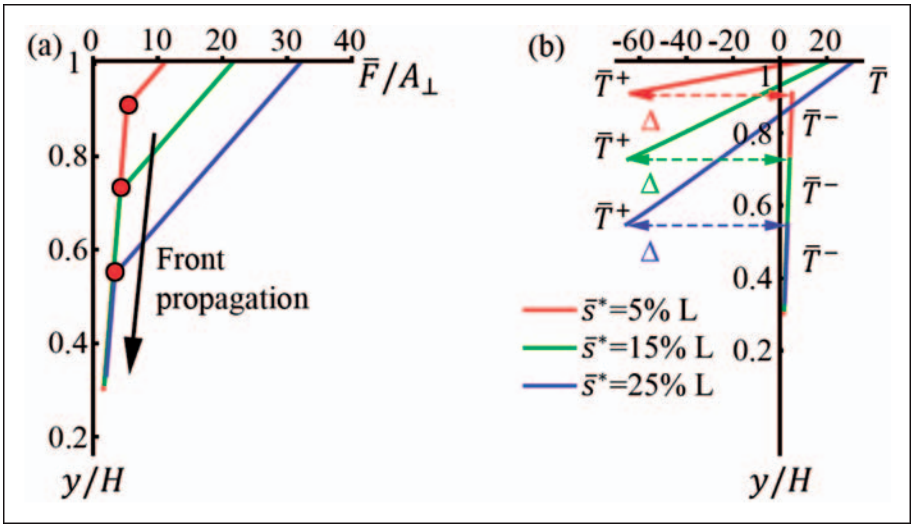

Figure 8. Change in the stressed state of the sample cross-section with flow propagation (a) in terms of normalized effective stress, (b) in terms of tension acting on the fibers. Both stresses are normalized by the weight of the dry sample $\rho^{-}gL$ over its cross-section $A_\perp$. The front position is shown with a red dot. Different colors correspond to different front positions shown on a legend. The vertical coordinate y changes from point of fixation H to the profile minima, which slightly shifts up during liquid penetration.

consequent higher vertical component of tension (see Figures 5(a) and 7(e)). When the sample reverses its motion towards the symmetrical configuration, the vertical force component decreases and the total tension again is almost equal its horizontal component.

Elasto-capillary effect in partially wet catenary

Elasto-capillary effect in freely suspended samples. When the sample is suspended freely, the value of the force F acting at each sample cross-section can be extracted from the shape of the sample profile for both wet and dry parts of the sample (see Equation 6) As discussed in above, in the dry part of the sample, this force distributes over the fibrous mesh of the loaded cross-section, whereas in the wet part, the fibers share the load with the filling liquid. Equations 1 and 2 can be re-written to give $T^{\pm} = F^{\pm}(s, s^*)/(A_\perp \cdot (1 - \varepsilon_\perp)) + P_l(s, s^*)\cdot \varepsilon_\perp/(1 - \varepsilon_\perp)$, provided that the pressure is equal to zero, $P_l(s, s^*) = 0$, in the empty part of the sample.

For the wet part of the material the pressure in the liquid column can be rewritten as

$$P_l = -P_c \cdot s/s^* + \rho_l g(H - y^+(s))(1 - s/s^*)$$

(Equation (7)). This pressure decreases from zero at the liquid source to $P_l = -P_c$ at the moving front. In terms of the tension that is experienced by fibers, the wetting liquid always acts to compress the fibrous mesh. The strongest compression occurs at the wetting front and depends on the capillary pressure build in the pores of the material. Therefore, the stressed state of the fibers in the wet part of the sample is the result of tension interplay caused by the weight of the sample stretching the fibers and compression caused by the capillary pressure. In the dry part of the sample, the fibers are always under tension. Figure 9(d) shows the tension distribution in a partially wet sample with $s^* = 0.3L$ for the geometrical parameters given in Table 1. Here Δ is a reduction of the tension on fibers at the moving front. One can see that the wet fibers experience a transition from tension at the suspension point to compression closer to the wicking front.

Evolution of stresses with front propagation. Figure 8(a) shows the dependence of the normalized average stress $\bar{F}/A_\perp$ on the vertical coordinate y of the sample cross-section, $y_{min} \le y \le H$, where the force is normalized by the weight of dry sample $\bar{F} = F/\rho^{-}gL$. The stress has two distinct regions. A sharp change of the slope indicates a transition from the wet to the dry part. As the figure shows, the average stress in the wet part increases as the wetting front propagates into the sample. In the dry part, the average stress remains nearly static. This behavior is similar to the downward wicking, for which this graph is plotted, into the vertically placed yarn.[15]

With the given analysis of the affective stress $\bar{F}/A_\perp$, we can apply Equation (2) to obtain the stress distribution in the fibrous matrix (Figure 8(b)) . The stresses on the fibers in the dry part are always tensile, and the stresses on the fibers in the wet part are lower, because the liquid supports the load. Owing to an additional capillary pressure, the fibrous matrix in the wet part

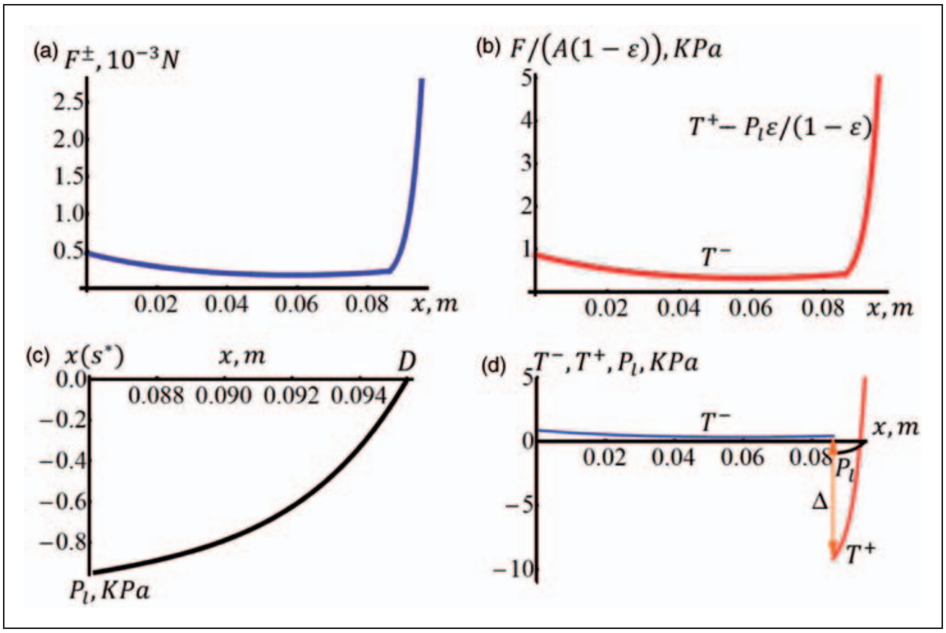

Figure 9. a) The distribution of tensile force $F^{\pm}$, acting upon the sample cross-section along the sample length (calculated using Equation (6)). (b) The distribution of tensile force F normalized by the total fiber area $A(1-\varepsilon)$ for samples saturation level $s^*/L = 0.3$. (c) Pressure distribution in the liquid column of length $s^* = 0.3\,L$ filling the sample. The pressure at the source ($x = D$) is equal to zero atmospheric pressure and the pressure at the front ($x = x(s^*)$) is equal to the capillary pressure. The size of the effective pores is taken to be $R_p = 152\,\mu$m. (d) The distribution of stresses $T^{\pm}$exerted on fibers along the sample and pressure distribution in the liquid column. The arrow indicates a pressure drop on the liquid front.

can be partially under tension and partially under compression (see Figure 8(b)). As expected, an addition of a heavy liquid increases the load on the fibrous matrix.

Estimates of the elasto-capillary effect. When the sample profile is known, the tensile forces $F^{\pm}$ acting on each sample cross-section can be immediately determined using Equations (1) and (2) (Figure 9(a)). Thus, the tensions hidden in the straight samples during the wicking experiments are manifested through deformations of the sagged samples. These deformations enable an estimation of not only the internal tensions, but also the elasto-capillary effect, since the capillary pressure is known. By simply combining Equations (1) and (2) and (6) and (7), the actual values of tensions on the fibers, T^{-} and T^{+} can be obtained: Figure 9 illustrates this stress analysis.

As we have discussed above, the fibers in the tested samples were densely packed to prevent buckling caused by the elasto-wetting effect. However, by tracking the change of the sample shape, it is possible to estimate the reduction in tension on fibers caused by the elasto-capillary effect. For example, for the experimental parameters given in Table 1, the maximum tension experienced by the fibers was approximately 9 kPa and was equal to the force acting at the minimum of the sample profile when the sample is completely wet. The maximum tension difference, $\Delta = P_c\varepsilon_{\perp}/(1-\varepsilon_{\perp})$, caused by the elasto-capillary effect during water wicking was estimated as $\Delta = 9.58$ kPa. We found that lightweight materials such as paper towels will almost always experience a transition from tension to capillarity-induced compression. Figure 9 shows the tensile stress b, the pressure distribution in the liquid column c and the tension on the fibers d when the liquid column reached $s = 0.3\,L$. The wet part of the sample experiences a transition from tension to compression, while the dry part of the sample remained stretched continuously.

Conclusions

In this paper, we have discussed the elasto-capillary effects in fibrous materials and analyzed the stresses in the Bernoulli problem of a freely hanging fabric when one end is brought into contact with a wetting liquid. We have analyzed in detail the evolution of tensile force acting on the fibers upon fabric wetting. We have determined that the elasto-capillary effect can be distinguished from other deformation effects, because of the stress distribution in partially wet fibrous materials has a peculiar form with a jump at the wetting front. The Bernoulli problem of a freely sagged fabric appears to be instructive and helpful for understanding the tension distribution in a two-dimensional self-reconfigurable material. We confirmed that the elasto-capillary effect in paper towels and similar flexible light-weight materials is significant.

Acknowledgement

The editorial assistance of Mr Godfrey Kimball of Clemson University is gratefully acknowledged.

Funding

We acknowledge the support from the National Science Foundation (grant numbers CMMI-0826067 and EFRI 0937985).

References

1. Scheidegger AE. *The physics of flow through porous media*, 3rd ed. Toronto: University of Toronto, 1974.
2. Terzaghi K. *Theoretical soil mechanics*. New York: Wiley, 1940.
3. Terzaghi K and Peck RB. *Soil mechanics in engineering practice*. New York: Wiley, 1948.
4. Wang H. *Theory of linear poroelasticity with applications to geomechanics and hydrogeology*. Princeton, NJ: Princeton University Press, 2000.
5. Nyoni AB and Brook D. Wicking mechanisms in yarns - the key to fabric wicking performance. *J Textile Inst* 2006; 97: 119–128.
6. Nyoni AB and Brook D. The effect of cyclic loading on the wicking performance of nylon 6.6 yarns and woven fabrics used for outdoor performance clothing. *Textile Res J* 2010; 80: 720–725.
7. Mustata A. Mechanical behaviour in the wet and dry stage of Romanian yarns made from flax and hemp. *Fibres Text East Eur* 2010; 18: 7–12.
8. Seo M, Wu HC, Chen J, Toomey CS and Backer S. Wear and fatigue of nylon and polyester mooring lines. *Textile Res J* 1997; 67: 467–480.
9. Roman B and Bico J. Elasto-capillarity: deforming an elastic structure with a liquid droplet. *J Phys Condensed Matter* 2010; 22: 493101.
10. Gopinath A and Mahadevan L. Elastohydrodynamics of wet bristles, carpets and brushes. *Proc R Soc A Math Phys Eng Sci* 2011; 467: 1665–1685.
11. Duprat C, Protière S, Beebe AY and Stone HA. Wetting of flexible fibre arrays. *Nature* 2012; 482: 510–513.
12. Bico J, Roman B, Moulin L and Boudaoud A. Elastocapillary coalescence in wet hair. *Nature* 2004; 432: 690.
13. Rossi MP, Gogotsi Y and Kornev KG. Deformation of carbon nanotubes by exposure to water vapor. *Langmuir* 2009; 25: 2804.
14. Wu X-F, Bedarkar A and Akhatov IS. Hydroelastic analysis of an axially loaded compliant fiber wetted with a droplet. *J Appl Phys* 2010; 108: 083518.
15. Monaenkova D and Kornev KG. Elastocapillarity: Stress transfer through fibrous probes in wicking experiments. *J Colloid Interface Sci* 2010; 348: 240–249.
16. Kisilak D. A new method of evaluating spherical fabric deformation. *Textile Res J* 1999; 69: 908–913.
17. Monaenkova D, Kornev KG and Andrukh T. Wicking of liquids into sagged fabrics. *Soft Matter*. in press, 2011.
18. Hearle JWS, Grosberg P and Backer S. *Structural mechanics of fibers, yarns, and fabrics*. New York: Wiley, 1969.
19. Bernoulli J. Lectures on the integral calculus, The first English translation of selections from Bernoulli's ground-breaking work of 1691–1692 identifying the curve formed by a hanging chain suspended at both ends, translated by William A. Ferguson, Jr (2004; accessed 28 December 2009).
20. Gordon JE. *Structures: Or, why things don't fall down*. New York: Penguin Books, 1978.
21. Flugge W. *Stresses in shells*. Berlin: Springer-Verlag, 1960.
22. Landau LD and Lifshitz EM. *Theory of elasticity*, 2nd ed. New York: Pergamon, 1970.
23. Freeman I. A general form of the suspension bridge catenary. *Bull Am Math Soc* 1925; 31: 425–429.
24. Klucakova M. Analysis of relationship between properties and behaviour of materials used and impregnation conditions of carbon-carbon composites. *Acta Materialia* 2005; 53: 3841–3848.
25. Callegari G, Tyomkin I, Kornev KG, Neimark AV and Hsieh YL. Absorption and transport properties of ultra-fine cellulose webs. *J Colloid Interface Sci* 2011; 353: 290–293.
26. Tsai C-C, Mikes P, Andrukh T, et al. Nanoporous artificial proboscis for probing minute amount of liquids. *Nanoscale* 2011; 3: 4685–4695.

Appendix 1

In our experiment, a fibrous sample (Mardi-Gras White, 709-2 Ply sheets, 22.3 cm × 27.9 cm, Georgia-Pacific Consumer Products) was suspended between two posts of equal height (see Figure 1(a)). The ends of the sample were held between two glass slides. The right end of the sample is extended from under the slide and is immersed in the Petri dish filled with a wetting liquid (water). A grid in the form of an array of marked lines with the 1 cm spacing was drawn on the material surface. The wet and dry parts of the sample had different optical contrast with a darker wet part. In order to observe the front position, a mirror was installed above the material in such a way that the camera (Diagnostic Instruments Inc., MI) was capable of simultaneous recording of the sample profile and the wetting front position as shown in Figure A1.

The ruler was placed in front of the sample at the left post and it was used as a reference. The fabric edge nearest to the camera and the ruler were sitting in the same plane. Therefore, the camera was focused on the nearest fabric edge and it traced the edge deflection simultaneously recording the front position from the mirrored image. The latter helped us to specify the

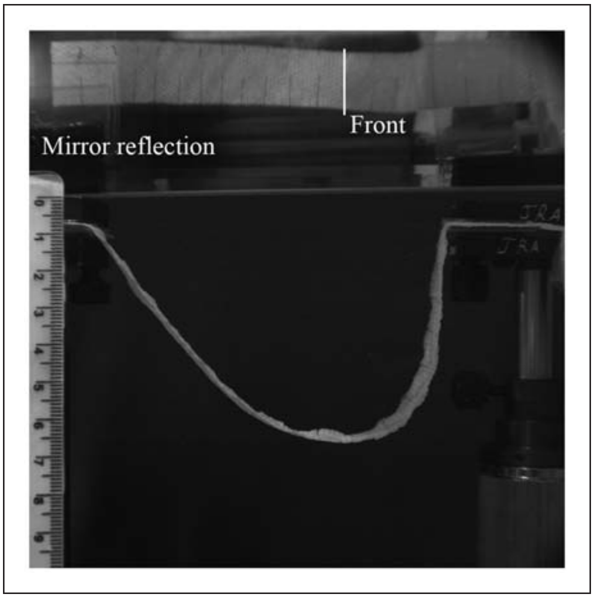

Figure A1. Side and top views of the freely-suspended suspended sample and its reflection in the mirror from the top of the sample. The wet part appears darker.

front position. The center of coordinate was placed at the visible lowest point on the left post of each image. The position of this point did not change during the experiment.

Notations

L length of the sample between suspension points
D distance between two posts
H height of the posts
h sample thickness
w width of the sample
k sample permeability
γ liquid surface tension
g acceleration due to gravity
R_p pore radius in the material
Δ stress jump between dry and wet parts
$\varepsilon_\perp$ trans-plane porosity of the material
$\varepsilon_{||}$ in-plane porosity of the material
F^-, F^+ in-plane tensile forces in the sample
$\bar{F}$ dimensionless force normalized by the weight of dry sample
$\sigma_\perp^-, \sigma_\perp^+$ in-plane stress acting over the sample edge
$T_\perp^-, T_\perp^+$ average normal tension experienced by each fiber
$\bar{T}^-$ dimensionless tension of dry band, normalized by the weight of the dry sample
$\bar{T}^+$ dimensionless tension of wet band, normalized by the weight of the wet sample
$F_x^\pm$ horizontal force components
$F_y^\pm$ vertical force components
$F(x_i, y_i)$ force at point (x_i, y_i)
$A_\perp$ area of the trans-plane cross-section
$A_\perp^p$ total area of pores in the trans-plane cross-section
$\sigma_{\|}^-, \sigma_{\|}^+$ trans-plane stress acting at the sample surface
$T_{\|}^-, T_{\|}^+$ average trans-plane tension experienced by each fiber
$A_{||}$ in-plane area of the sample
$A_{||}^{\mathrm{p}}$ total in-plane area of the pores
P_l pressure in the liquid
P_c capillary pressure in the liquid
s arclength along the sample profile, counted from the suspension point
s^* front position counted from the suspension point
a^-, a^+ catenary shape factor
ρ^-, ρ^+ linear density of the dry/wet material
$\left(x_{min}^\pm, Y_{min}^\pm + a^\pm\right)$ coordinates of the catenary minimum
$(y(s), x(s))$ Cartesian coordinates corresponding to arclength s
$\left(x^\pm, y^\pm\right)$ set of coordinates, describing the wet/dry band
s_{min} arclength, measured along the sample from the suspension point to the profile minimum
s_i arclength, measured along the sample from the suspension point to point (x_i, y_i)
$\bar{x}, \bar{y}, \bar{s}$ dimensionless lengths, normalized by the total length L of the sample

Superscripts

$-$ dry part of the sample
$+$ refers to the wet part of the sample